Korean J. Chem. Eng., 36(8), 1371-1376 (2019)
DOI: 10.1007/s11814-019-0320-0

pISSN: 0256-1115
eISSN: 1975-7220

Atmospheric-pressure floating electrode-dielectric barrier discharge with flexible electrodes: Effect of conductor shapes

Jun-Hyun Kim*, Jin-Su Park, Yong-Seon Shin**, and Chang-Koo Kim**,†**

*Institute of NT-IT Fusion Technology, Ajou University, 206 Worldcup-ro, Yeongtong-gu, Suwon 16499, Korea
**Department of Chemical Engineering and Department of Energy Systems Research, Ajou University, 206 Worldcup-ro, Yeongtong-gu, Suwon 16499, Korea
(*Received 7 April 2019 • accepted 1 June 2019*)

Abstract−The plasma characteristics of atmospheric-pressure floating electrode-dielectric barrier discharges (FE-DBDs), which comprised flexible electrodes and were able to generate a plasma along the curvature of skin, were investigated using Cu conductors with various shapes in the flexible powered electrode. These Cu conductors have similar areas but different contour lengths and the shapes of a square, a dumbbell, a star, and a zigzag pattern. The optical intensity and electron temperature of the atmospheric-pressure FE-DBDs increased with the contour length of the conductor used in the flexible powered electrode. This behavior is explained in terms of the changes in the strength of the electric field with the contour length of the conductor, implying that the plasma properties of atmospheric-pressure FE-DBDs with flexible electrodes can be controlled by modulating the contour length or the shape of the electrical conductor in the flexible powered electrode. These results are expected to contribute to the development of an atmospheric-pressure FE-DBD system for plasma medicine.

Keywords: Dielectric Barrier Discharge, Plasma, Flexible Electrode, Conductor, Contour Length, Plasma Medicine

INTRODUCTION

A plasma is a partially ionized gas consisting of electrons and ions (positive and negative) in abundant un-ionized neutrals. Plasmas can be classified into low-pressure (lower than atmospheric pressure) and atmospheric-pressure based on the pressure at which they are generated. Low-pressure plasmas are mainly used to pattern high-aspect-ratio features in the fabrication of a variety of devices, such as microelectronics, microelectromechanical systems, and optoelectronics [1-6]. Stable plasmas can be easily achieved at low pressures, but the use of a vacuum system is indispensable for the generation of low-pressure plasmas. This makes them expensive and complicated to use. On the other hand, the setups for atmospheric-pressure plasma systems are not expensive because they do not require vacuum-generating equipment. In addition, continuous processing is possible for atmospheric-pressure plasmas, allowing for fast processing speeds.

Plasma medicine has drawn much attention because it has been reported that reactive oxygen species (ROS) and reactive nitrogen species (RNS) generated from atmospheric-pressure plasmas could enhance sterilization, wound healing, tissue generation, etc. [7-11]. These ROS and RNS, such as superoxide (O_2^-), hydrogen peroxide (H_2O_2), hydroxyl radical (OH), ozone (O_3), nitric oxide (NO), nitrogen dioxide (NO_2), and peroxynitrite ($ONOO^-$), also play important roles in the immune systems of living organisms (both in animals and plants).

Atmospheric-pressure plasmas used in medical applications should not cause the thermal deterioration of living tissue so that human skin can safely come into contact with them. For that purpose, it is necessary to use "cold" or "non-thermal" atmospheric-pressure plasmas. Plasma jets and dielectric barrier discharges (DBDs) are representative types of cold atmospheric-pressure plasmas currently in use in plasma medicine.

Plasma jets [12-14] typically consist of two concentric electrodes through which a gas flow is introduced. A plasma is ignited in a capacitively coupled manner by applying radio-frequency power to the inner electrode and then exits through a nozzle at very high speed. In plasma jets, plasma chemistry can be modulated because various gases can be discharged. In addition, the flux of the reactive species incident on the substrate is very high owing to their emission through the nozzle. However, the small spot size (several mm) of plasma exposure achieved using plasma jets is disadvantageous if uniform treatment of a large area is required.

DBDs [15-17] consist of two electrodes covered with dielectric layers. Depending on the configuration, one or both of the electrodes are covered with dielectric materials. Plasmas are generated between the electrodes by applying an alternating current (AC) or pulsed power to one of the electrodes. These plasmas can then be ignited by replacing the grounded electrode with human skin. These are called floating electrode-dielectric barrier discharges (FE-DBDs) [18-20]. DBDs can be sustained without the introduction of gas and offer a much larger plasma exposure area than plasma jets.

When considering using atmospheric-pressure plasmas for healing wounds on human skin, DBDs are appropriate because they provide large-area discharges. In addition, DBDs with flexible electrodes could be effective for the generation of a plasma along the

†To whom correspondence should be addressed.
E-mail: changkoo@ajou.ac.kr

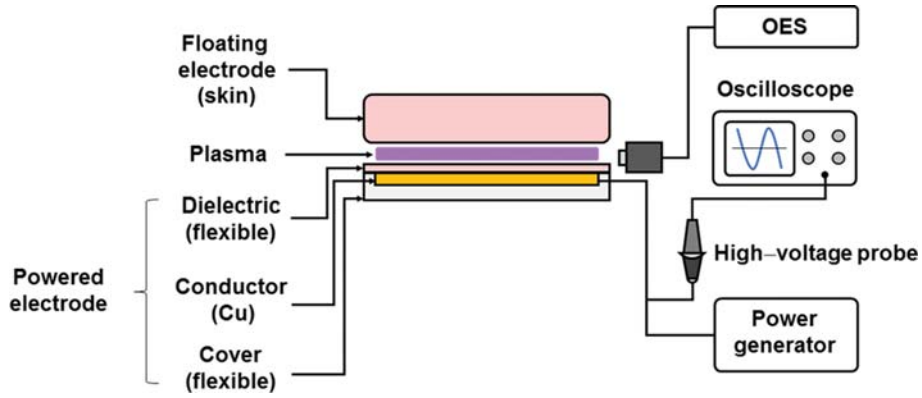

Fig. 1. Schematic of an atmospheric-pressure FE-DBD system with a flexible electrode.

curvature of the skin. The application of DBDs with flexible electrodes in plasma medicine has been rarely reported.

Recently, we reported on the development of an atmospheric-pressure FE–DBD system with flexible electrodes and showed that its plasma characteristics could be controlled by modulating the dielectrics and voltage applied to the flexible powered electrode [21]. As an extension of the previous study, we here examined the plasma characteristics of an atmospheric-pressure FE-DBD for flexible powered electrodes using electrical conductors of various shapes. The shapes of the conductors were chosen to have similar surface areas but different contour lengths. Materials having high electrical conductivity such as graphene can be used as a conductor for flexible electrodes [22-30]. In this study, copper (Cu) was used as a conductor because various shapes of Cu can be relatively easily obtained using electroless deposition. The plasma properties were determined by investigating the changes in the optical intensities of the RNS and ROS generated in the atmospheric-pressure FE-DBD for various conductor shapes. The electron temperatures were extracted from the optical intensities of the plasma, and their dependence on the shape of the conductor in the flexible powered electrode was also examined.

EXPERIMENTAL

Fig. 1 shows a schematic of an atmospheric-pressure FE-DBD system with a flexible electrode. The atmospheric-pressure FE-DBD system used consisted of a floating electrode (which was skin) and a powered electrode. Pig skin, which has similar characteristics to human skin, was used as the floating electrode in this study. The powered electrode (50×50 mm^2 in size) consisted of a stack comprising a flexible cover, an electrical conductor, and a flexible dielectric. This structure made the powered electrode flexible and bendable, allowing it to accommodate to the shape of the floating electrode. The flexible cover made of polydimethylsiloxane (PDMS) with a thickness of 5 mm was used to inhibit plasma ignition toward the direction opposite to the floating electrode. The flexible dielectric used was a 0.1-mm-thick polyethylene terephthalate (PET) film, which has good flexibility. A thin copper (Cu) film with a thickness of 450 μm, which was used as the electrical conductor to receive the external power, was placed between the flexible cover and the dielectric. Cu films with various shapes were plated on the PET dielectric to examine the effect of conductor shape on the plasma characteristics of the atmospheric-pressure FE-DBD system.

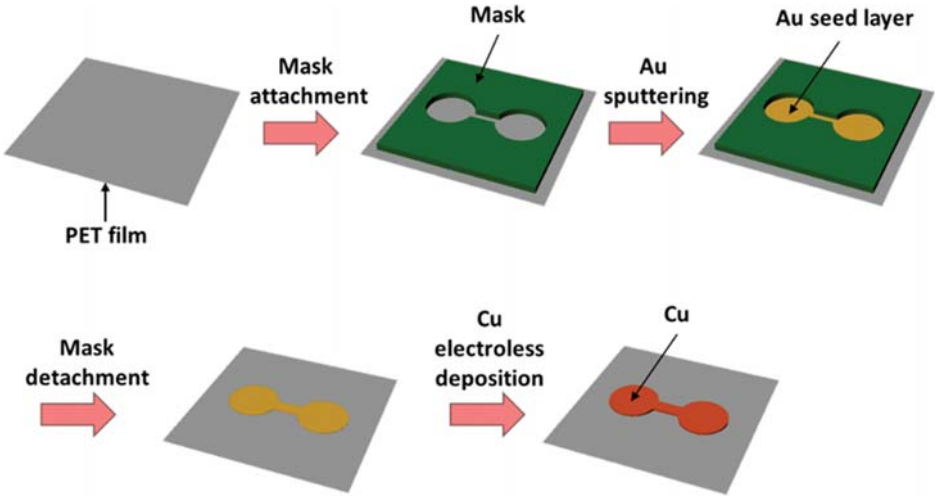

Fig. 2. Schematic of the Cu conductors fabricated on the PET film.

Cu was plated on the PET film via an electroless deposition method. Electroless deposition of Cu on a dielectric material (such as PET) requires a conductive seed layer on the dielectric to initiate the process. Conductive seed layers such as palladium (Pd) and platinum (Pt) are usually formed by dipping the dielectric into a bath containing precursors of the seed layers [31,32]. However, these chemicals are very reactive, severely damaging any PET that gets in contact with them. In this work, a seed layer was formed on the PET film via sputtering instead of dipping into a chemical bath.

Fig. 2 shows a schematic of the fabrication of Cu conductors on a PET film. A patterned mask was placed on the PET film to achieve the selective formation of a seed layer on specific regions. The mask was fabricated using a fused-filament 3D printer (MakerBot Replicator 2, MakerBot Industries). A gold (Au) seed layer was deposited on the unmasked area via sputtering using an ion coater (KIC-IA, COXEM). After Au sputtering, the mask was detached from the PET film, and the specific shape (dumbbell in this figure) of the seed layer remained. Then, a Cu film was electrolessly deposited on the seed layer. The electroless deposition of this Cu film was carried out using copper sulfate ($CuSO_4 \cdot 5H_2O$). Formaldehyde (HCHO) and ethylenediaminetetraacetic acid (EDTA) were used as reducing and complexing agents, respectively. The complexing agent prevented spontaneous metal reduction and precipitation in the solution [33,34]. The solution was prepared by dissolving the chemicals in deionized water. The pH of the solution was adjusted to 12 using sodium hydroxide (NaOH). Electroless deposition was carried out at 80 °C for 45 minutes to fabricate a 450-μm-thick Cu film. Via this process, the shape of the mask pattern was transferred to Cu on the PET film.

Fig. 3 shows the various shapes (square, dumbbell, star, and zigzag) of the Cu conductors fabricated using the abovementioned method and their dimensions. The shapes of the Cu conductors were chosen to have similar surface areas but different contour lengths; the values are listed in Table 1.

Table 1. Surface areas and contour lengths of the various shapes of the Cu conductors in the flexible powered electrode

	Area (mm^2)	Contour length (mm)
Square	930	122
Dumbbell	930	151
Star	960	372
Zigzag	969	652

AC power (frequency of 25 kHz and peak-to-peak voltage of 15 kV) was applied to the Cu conductors by using a power generator. The voltage was measured with an oscilloscope (Tektronix, RDS3034) equipped with a high-voltage probe. The optical intensity of the plasmas generated between the flexible powered electrode and the floating electrode (skin) was measured with an optical emission spectroscope (OES, GetSpec, 2048TEC).

RESULTS AND DISCUSSION

Fig. 4 shows the OES spectra of the atmospheric-pressure FE-DBDs having Cu conductors with various shapes in the flexible powered electrode. It can be seen that the peaks for nitrogen and oxygen radicals appeared at wavelengths ranging from 300 to 450 nm and from 777 to 845 nm, respectively. When a plasma was ignited at atmospheric pressure without introducing oxygen, its composition was dominated by nitrogen states because the transition energy from the ground state to excited states for nitrogen is lower than that of oxygen [35]. The OES measurements of the atmospheric pressure FE-DBD after 20 times bending of the flexible powered electrode were also made, and their OES spectra were exactly identical to those without bending (not shown here).

To better observe the changes in the optical intensities of the plasmas according to the shape of the conductor used, the 359-nm peaks, which were the highest nitrogen peaks in the OES spectra measured, were compared. Fig. 5 shows the optical intensity of the peaks at a wavelength of 359 nm in the OES spectra as a function of con-

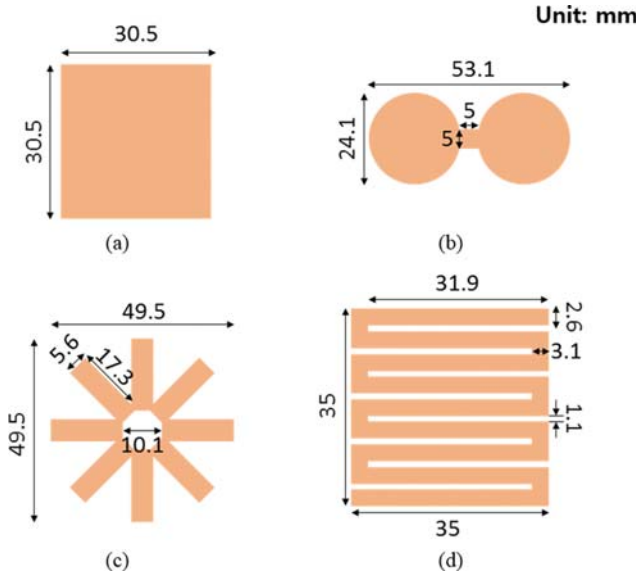

Fig. 3. Various shapes of the Cu conductors used in this study and their dimensions. (a) Square, (b) dumbbell, (c) star, and (d) zigzag.

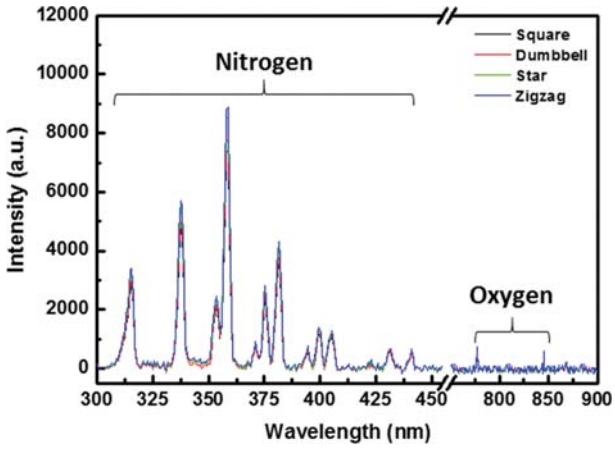

Fig. 4. OES spectra of the atmospheric-pressure FE-DBDs with Cu conductors with various shapes in the flexible powered electrode.

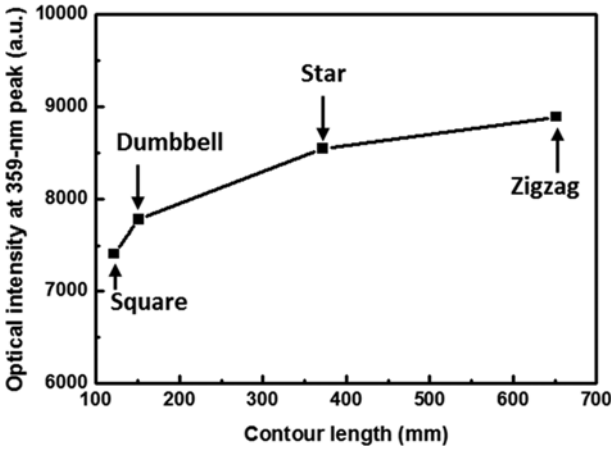

Fig. 5. Optical intensity at the 359-nm peak of the atmospheric-pressure FE-DBDs as a function of the contour length of the conductors in the flexible powered electrode.

tour length of the conductor in the flexible powered electrodes. The optical intensity of the atmospheric-pressure FE-DBDs increased with the contour length of the conductor. In addition, the dumbbell-shaped conductor (contour length=151 mm) yielded a higher optical intensity than the square-shaped conductor (contour length= 122 mm), although their surface areas were identical (930 mm^2). This suggests that contour length may be a characteristic parameter to investigate the effect of the shape of the conductor on the plasma properties of atmospheric-pressure FE-DBDs.

The change in the plasma characteristics with the shape of the electrode can also be found in several DBD systems. Schwabedissen et al. investigated the formation of ozone using a DBD system, and showed that the ozone production rates increased with increasing contour length of the electrode [36]. Fujishima examined DBD systems having a single electrode or multiple electrodes with the same area as the single electrode for ozone generation [37]. He obtained higher discharge power and ozone concentration under the DBD system having multiple electrodes. This was explained by the formation of strong electric field at the edge of the electrode.

As shown in Fig. 5, the optical intensity of the plasmas generated in the atmospheric-pressure FE-DBD system with flexible electrodes was dependent on the contour length of the conductor in the flexible powered electrode, implying that the energy of the electrons in the plasma was affected by the contour length of the conductor. The energy of electrons is usually represented by the electron temperature. In a plasma, active species, such as RNS and ROS, are produced by collisions between electrons and molecules (e.g., nitrogen or oxygen). Therefore, higher electron temperatures increase the electron impact rate and correspondingly result in more active species [38,39]. In addition, an increase in the electron temperature leads to an increase in the optical intensity of the plasma [40].

In low-pressure plasmas, electron temperature can be directly measured using the so-called Langmuir probe. However, it is difficult to apply this probe technique at atmospheric pressures because the large frequency of electron-neutral collisions causes heat load and high-frequency noise [41]. As an alternative to direct probe measurements, the electron temperature of an atmospheric-pressure plasma can be obtained via indirect methods, one of which is the Boltzmann plot method [41,42].

The Boltzmann plot method allows one to obtain the electron temperature of a plasma using the relative intensity of optical line spectra that exhibit relatively large differences. Starting with a Boltzmann distribution, the electron temperature can be expressed in terms of the wavelength and intensity of the light emitted from a plasma, as given in Eq. (1):

$$\ln\left(\frac{\lambda_{ki}I_{ki}}{A_{ki}g_k}\right) = -\frac{E_k}{k\,T_e} + c, \tag{1}$$

where T_e is the electron temperature, λ_{ki} and I_{ki} are the wavelength and the intensity, respectively, of the emitted light for a transition from a higher state k to a lower state i, A_{ki} is the probability of transition from state k to state i, g_k is the statistical weight of state k, E_k is the energy level of state k, k is the Boltzmann constant (1.38×10^{-23} J/K), and C is a constant. Here, A_{ki} and g_k were obtained from a database provided by the National Institute of Standards and Technology [43,44]. By plotting $\ln\left(\frac{\lambda_{ki}I_{ki}}{A_{ki}g_k}\right)$ on the vertical axis versus E_k on the horizontal axis, the electron temperature can be determined from the slope of the resulting straight line.

Fig. 6 shows the Boltzmann plot of the atmospheric-pressure FE-DBDs with conductors of various shapes in the flexible powered electrode. The Boltzmann plot was obtained using Eq. (1) and the nitrogen radical peaks at wavelengths of 317.7, 340.8, 345.1, 359.4, 367.6, 377.6, 383.0, 393.0, 397.7, 404.7, 431.9, and 441.3 nm in the OES spectra of the plasmas.

We propose that contour length could be a characteristic parameter to investigate the effects of the shape of the conductor on the plasma properties of atmospheric-pressure FE-DBDs. To examine the dependence of electron temperature on the shape of the conductor, the obtained electron temperatures were compared for various contour lengths of the conductor in the flexible powered electrode. The results are shown in Fig. 7, where it can be seen that the

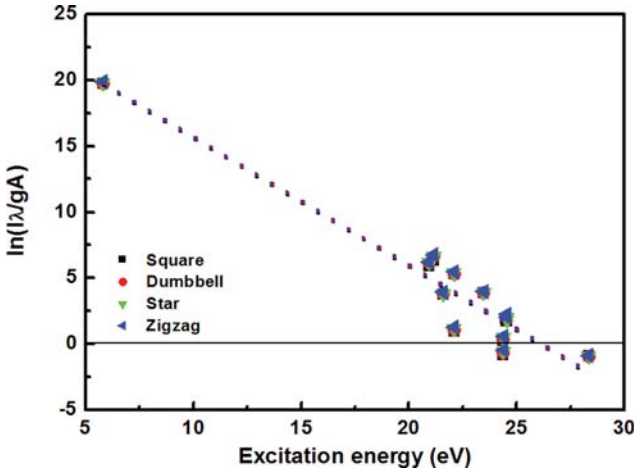

Fig. 6. Boltzmann plots of the atmospheric-pressure FE-DBDs with conductors with various shapes in the flexible powered electrode.

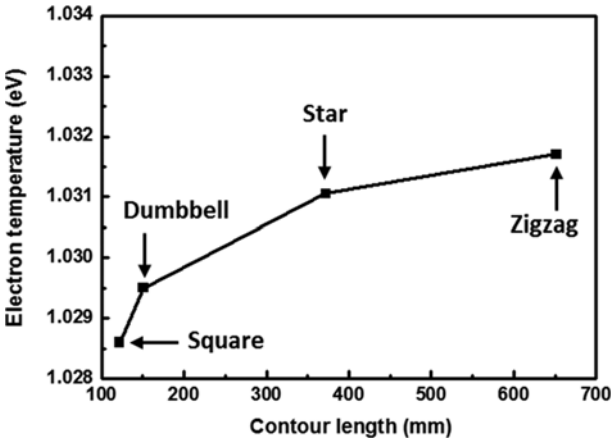

Fig. 7. Electron temperature of the atmospheric-pressure FE-DBDs as a function of contour length of the conductors of the flexible powered electrode.

electron temperature of the atmospheric-pressure FE-DBD systems increased with the contour length of the conductor. This behavior exhibits the same relationship as that between the optical intensity of the peak at a wavelength of 359 nm and the contour length of the conductor (see Fig. 5). When external power is applied to the conductor, a strong electric field forms on its edges. Therefore, the electric field gets stronger as the contour length of the conductor increases. Because electrons accumulate energy while travelling in an electric field, they acquire more energy as the electric field increases. This leads to an increase in electron temperature as the contour length of the conductor increases, indicating that the plasma properties of an atmospheric-pressure FE-DBD having flexible electrodes can be controlled by changing the contour length (i.e., shape) of the electrical conductor in the flexible powered electrode.

CONCLUSIONS

An atmospheric-pressure FE-DBD system with electrical conductors of various shapes in the flexible powered electrode was developed and its plasma characteristics were investigated. Thin Cu films in the shapes of a square, a dumbbell, a star, and a zigzag pattern with similar surface areas, but different contour lengths, were used as conductors in the flexible powered electrode of the system and were electrolessly deposited on the PET dielectric film.

For all the shapes of the conductors in the flexible powered electrode, the OES spectra of the atmospheric-pressure FE-DBDs showed that both nitrogen and oxygen radical peaks appeared and that the composition of the plasmas was dominated by nitrogen. The optical intensity of the plasmas increased with the contour length of the conductors even though their surface areas were nearly identical, implying that contour length could be a characteristic parameter to investigate the effect of the shape of the conductor on the plasma properties of atmospheric-pressure FE-DBDs. The electron temperatures of the atmospheric-pressure FE-DBDs, which were obtained using the Boltzmann plot method, also increased with the contour length of the conductor in the flexible powered electrode. This occurred because, as the contour length of the conductor increased, the electric field got stronger, in turn causing the electrons to acquire more energy.

This study reveals that the plasma properties of an atmospheric-pressure FE-DBD with flexible electrodes can be controlled by changing the contour length of the electrical conductor in the flexible powered electrode.

ACKNOWLEDGEMENTS

This work was supported by the National Research Foundation of Korea (NRF) grant funded by the Korea government (MEST) (Grant No. 2018R1A2B6002410) and the GRRC program of Gyeonggi province (GRRC AJOU 2016B03, Photonics-Medical Convergence Technology Research Center).

REFERENCES

1. M. Schaepkens, G. S. Oehrlein, C. Hedlund, L. B. Jonsson and H. O. Blom, *J. Vac. Sci. Technol. A*, **16**, 3281 (1998).
2. J.-H. Kim, S.-W. Cho, C. J. Park, H. Chae and C.-K. Kim, *Thin Solid Films*, **637**, 43 (2017).
3. S.-W. Cho, C.- K. Kim, J.-K. Lee, S. H. Moon and H. Chae, *J. Vac. Sci. Technol. A*, **30**, 051301-1 (2012).
4. T. H. Lee, B. R. Lim, K. J. Yong, W. S. Kwon and M. W. Park, *Korean J. Chem. Eng.*, **34**, 2502 (2017).
5. S. H. Ji, W. S. Jang, J. W. Son and D. H. Kim, *Korean J. Chem. Eng.*, **35**, 2474 (2018).
6. J. H. Choi, S. J. Kim, H. T. Kim and S. M. Cho, *Korean J. Chem. Eng.*, **35**, 1348 (2018).
7. G. Fridman, G. Friedman, A. Gutsol. A.B. Shekhter, V. N. Vasilets and A. Fridman, *Plasma Process. Polym.*, **5**, 503 (2008).
8. J. Ehlbeck, U. Schnabel, M. Polak, J. Winter, T. von Woedtke, R. Brandenburg, T. von dem Hagen and K.-D. Weltmann, *J. Phys. D: Appl. Phys.*, **44**, 013002-1 (2011).
9. D. B. Graves, *J. Phys. D: Appl. Phys.*, **45**, 206330-1 (2012).
10. Z. Xiong, J. Roe, T. C. Grammer and D. B. Graves, *Plasma Process. Polym.*, **13**, 588 (2016).
11. K.-D. Weltmann and T. von Woedtke, *Plasma Phys. Control. Fusion*, **59**, 014031-1 (2017).
12. J. F. Kolb, A.-A. Mohamed, R. O. Price, R. J. Swanson, A. Bowman, R. L. Chiavarini, M. Stacey and K. H. Schoenbach, *Appl. Phys. Lett.*, **92**, 241501-1 (2008).
13. X. P. Lu, Z. H. Jiang, Q. Xiong, Z. Y. Tang and Y. Pan, *Appl. Phys. Lett.*, **92**, 151504-1 (2008).
14. H. W. Lee, S. H. Nam, A. H. Mohamed, G. C. Kim and J. K. Lee, *Plasma Process. Polym.*, **7**, 274 (2010).
15. U. Kogelschatz, *Plasma Chem. Plasma Process.*, **23**, 1 (2003).
16. M. J. Pavlovich, Z. Chen, Y. Sakiyama, D. S. Clark and D. B. Graves, *Plasma Process. Polym.*, **10**, 69 (2013).
17. X. Pei, J. Liu, Y. Xian and X. Lu, *J. Phys. D: Appl. Phys.*, **47**, 145204-1 (2014).
18. G. Fridman, M. Peddinghaus, H. Ayan, A. Fridman, M. Balasubramanian, A. Gutsol, A. Brooks and G. Friedman, *Plasma Chem. Plasma Process.*, **26**, 425 (2006).
19. G. Fridman, A. Shereshevsky, M. M. Jost, A. D. Brooks, A. Fridman, A. Gutsol, V. Vasilets and G. Friedman, *Plasma Chem. Plasma Pro-*

cess., **27**, 163 (2007).
20. N. Y. Babaeva and M. J. Kushner, *J. Phys. D: Appl. Phys.*, **43**, 185206-1 (2010).
21. J.-H. Kim, C. J. Park and C.-K. Kim, *Korean Chem. Eng. Res.*, **57**, 432 (2019).
22. C. Liang, H. Qiu, Y. Han, H. Gu, P. Song, L. Wang, J. Kong, D. Cao and J. Gu, *J. Mater. Chem. C*, **7**, 2725 (2019).
23. Y. Huangfu, C. Liang, Y. Han, H. Qiu, P. Song, L. Wang, J. Kong and J. Gu, *Compos. Sci. Technol.*, **169**, 70 (2019).
24. Y. Huangfu, K. Ruan, H. Qiu, Y. Lu, C. Liang, J. Kong and J. Gu, *Compos. Pt. A-Appl. Sci. Manuf.*, **121**, 265 (2019).
25. Y. Kang, C. Wang, Y. Qiao, J. Gu, H. Zhang, T. Peijs, J. Kong, G. Zhang and X. Shi, *Biomacromolecules*, **20**, 1765 (2019).
26. X. Dai, Y. Du, J. Yang, D. Wang, J. Gu, Y. Li, S. Wang, B. B. Xu and J. Kong, *Compos. Sci. Technol.*, **174**, 27 (2019).
27. K. Ruan, Y. Guo, Y. Tang, Y. Zhang, J. Zhang, M. He, J. Kong and J. Gu, *Compos. Commun.*, **10**, 68 (2018).
28. Y. Liu, M. Yao, L. Zhang and Z. Niu, *J. Energy Chem.*, **38**, 199 (2019).
29. Y. Zhao, J. Wang, C. Ma, L. Cao and Z. Shao, *Chem. Eng. J.*, **370**, 536 (2019).
30. A. Pedico, A. Lamberti, A. Gigot, M. Fontana, F. Bella, R. Rivolo, M. Cocuzza and C. F. Pirri, *ACS Appl. Energy Mater.*, **1**, 4440 (2018).
31. W. L. Goh, K. T. Tan, M. S. Tse and K. Y. Liu, *Int. J. Mod. Phys. B*, **16**, 197 (2002).
32. J. P. O'Kelly, K. F. Mongey, Y. Gobil, J. Torres, P. V. Kelly and G. M. Crean, *Microelectron. Eng.*, **50**, 473 (2000).
33. S. M. S. I. Dulal, T. H. Kim, H. Rhee, J. Y. Sung and C.-K. Kim, *J. Alloy. Compd.*, **467**, 370 (2009).
34. T. H. Kim, S. M. S. I. Dulal, C. H. Park, H. Y. Chae, and C.-K. Kim, *Surf. Coat. Technol.*, **202**, 4861 (2008).
35. P. Baroch, N. Saito and O. Takai, *J. Phys. D: Appl. Phys.*, **41**, 085207-1 (2008).
36. A. Schwabedissen, P. Lacinski, X. Chen and J. Engemann, *Contrib. Plasma Phys.*, **47**, 551 (2007).
37. T. Fujishima, *J. Int. Council Elec. Eng.*, **8**, 99 (2018).
38. D. Bose, S. Rauf, D. B. Hash, T. R. Govindan and M. Meyyappan, *J. Vac. Sci. Technol. A*, **22**, 2290 (2004).
39. N. Itagaki, S. Iwata, K. Muta, A. Yonesu, S. Kawakami, N. Ishii and Y. Kawai, *Thin Solid Films*, **435**, 259 (2003).
40. M. W. Ahmed, Md. S. Rahman, S. Choi, U. Shaislamov, J.-K. Yang, R. Suresh and H.-J. Lee, *Appl. Sci. Converg. Technol.*, **26**, 118 (2017).
41. N. Ohno, M. A. Razzak, H. Ukai, S. Takamura and Y. Uesugi, *Plasma Fusion Res.*, **1**, 028-1 (2006).
42. D. Xiao, C. Cheng, J. Shen, Y. Lan, H. Xie, X. Shu, Y. Meng, J. Li and P. K. Chu, *J. Appl. Phys.*, **115**, 033303-1 (2014).
43. http://physics.nist.gov/PhysRefData/ASD/index.html.
44. J. J. Camacho, J. M. L. Poyato, L. Díaz and M. Santos, *J. Phys. B: At. Mol. Phys.*, **40**, 4573 (2007).